Measurements of the complex plasma loading impedance of the magnetosonic cavity modes

D. Q. Hwang[a] and R. W. Gould

California Institute of Technology, Pasadena, California 91109
(Received 23 May 1979; accepted 20 November 1979)

The complex plasma loading impedance of the fast magnetosonic wave in the Caltech tokamak has been investigated at low power (between 10 and 300 W). The magnetosonic cavity modes are observed both as voltage maxima at the output of a six-turn receiving probe, and as maxima in the input resistance of the transmitting antenna. When the real and imaginary parts of the measured plasma loading impedance are plotted in the complex impedance plane, the resulting curves are approximately circles, indicating a resonance phenomenon. The observed plasma loading resistance at the various cavity modes is as high as 3 to 4 times the basic antenna resistance ($\sim 0.4\ \Omega$). This means that efficient energy coupling into the tokamak and low losses in the antenna system are possible. The estimated cavity Q's are between 400 and 700.

I. INTRODUCTION

Due to the decrease in plasma resistance with increasing plasma temperature, the Ohmic heating of a tokamak must be supplemented by other means of auxiliary heating. Currently, the two major methods proposed for heating a tokamak are neutral beam injection heating and radio frequency wave heating. Although neutral beam heating has enjoyed a great deal of success in heating present experimental tokamaks,[1] there are still many unanswered questions concerning its penetration and heating efficiency in heating the bulk of the ion distribution in a reactor-size tokamak. The use of radio frequency electromagnetic waves to heat a plasma has been proposed since the early days of plasma physics. Electromagnetic waves can be used to heat the various components in a multispecies plasma. In a two-component plasma, such as a (50-50) D-T mixture, wave heating can be used to selectively heat either of the two ion species or the electrons.

One of the rf heating methods is the use of the magnetosonic wave. The attractive feature of this method is that the wave energy should couple directly to the ions when the second harmonic cyclotron layer is inside the tokamak. In a multicomponent plasma, each ion species can be individually heated by selecting the rf frequency corresponding to the ion cyclotron frequency of the particular species. The theoretical aspects of magnetosonic heating have been treated by Stix,[2] and later by Adam and Samain,[3] Perkins *et al.*,[4] Hosea *et al.*,[5] Paoloni,[6] Swanson,[7] and Jacquinot *et al.*[8] The magnetosonic wave was first observed by Hooke *et al.*[9] and further studied by Swanson *et al.*[10] and Chung and Rothman.[11] The early attempts to use the magnetosonic cavity modes to heat tokamak plasma were performed in the TM-1-VCH tokamak and the TO-1 tokamak.[12,13] Later, the properties of the magnetosonic cavity modes were studied in greater detail in experiments on the ST, ATC, and TFR tokamaks.[14-16]

In this paper, we present the experimental results of magnetosonic wave generation, using a small loop antenna, in a tokamak plasma. Special attention is given to the measurement of the complex plasma loading impedance at the cavity modes. The experimental results confirm that the magnetosonic eigenmodes are indeed cavity resonance effects. The complex plasma loading impedance contains the information needed to match the rf generator impedance to the antenna in the presence of a cavity mode. Careful design of the antenna and the impedance matching network is found to be necessary for efficient energy coupling to the plasma and proper matching of the generator impedance to the antenna at a cavity mode. For the double-turn loop antenna used in the experiments, the wave generation efficiency is found to be as high as 80%. Finally, data showing the antenna being matched to a cavity mode where the maximum amount of power is delivered to the plasma are presented.

II. THEORY OF MAGNETOSONIC CAVITY MODES AND ANTENNA-CAVITY COUPLING

A. Cold plasma theory

The propagation of the magnetosonic wave in a tokamak can be described reasonably well by approximating the toroidal vacuum chamber by a cylinder and assuming that the plasma is cold, collisionless, and axially magnetized with a uniform magnetic field. Terms of order (m_e/m_i) in the plasma dielectric tensor ϵ, where m_e and m_i are the electron and ion masses, respectively, can be neglected. The propagation frequency of the wave is taken to be near the ion cyclotron frequency ω_{ci}, which is much smaller than the electron cyclotron frequency ω_{ce} and the electron plasma frequency ω_{pe}. The resulting dispersion for the magnetosonic wave is

$$k^2 = \frac{\Omega_i^2 \omega_{ci}^2}{V_A^2(1-\Omega_i^2)} - \frac{T^2}{2} + \left[\left(\frac{T^2}{2}\right)^2 + \left(\frac{\Omega_i^3 \omega_{ci}^2}{V_A^2(1-\Omega_i^2)}\right)^2\right]^{1/2}, \quad (1)$$

where T and k are the radial and axial components of the wave vector, Ω_i is ω/ω_{ci}, $V_A = B_0/(\mu_0 m_i n_i)^{1/2}$ is the Alfvén velocity in the plasma, and n_i is the ion number density.

A consequence of the propagation frequency being much smaller than the electron plasma frequency is that E_z is small. For our calculation, E_z is assumed to be zero. The solution of the axial magnetic field H_z is

[a] Present address: Plasma Physics Laboratory, Princeton University, Princeton, N. J. 08544.

 0031-9171/80/030614-10$00.90

$$H_z = H_0 J_m(Tr)\exp[j(\omega t - m\theta - kz)]\,, \tag{2}$$

where J_m is an integer-order Bessel function.

The boundary condition at the tokamak wall ($E_\theta = H_r = 0$) can be written

$$TaJ'_m(Ta) + (\gamma_2/\gamma_1)mJ_m(Ta) = 0\,, \tag{3}$$

where $\gamma_1 = k^2 - \omega^2\mu_0\epsilon_\perp$, $\gamma_2 = \omega^2\mu_0\epsilon_\times$, m is the poloidal mode number, and $\epsilon_\perp \cong \epsilon_0\omega_{pi}^2/(\omega_{ci}^2 - \omega^2)$ and $\epsilon_\times \cong (\omega/\omega_{ci})\epsilon_\perp$ are the components the dielectric tensor of a cold magnetized plasma.

Each of these cavity modes is identified by a set of mode numbers (l,m,N), where l is the radial mode number, m is the poloidal mode number, and N is the axial mode number.

The cutoff condition, i.e., $k = 0$, for the various modes is very useful both as a guide to the general trends of the dispersion curves in the density versus frequency plane and in the estimation of the cavity Q. For $\omega/\omega_{ci} > 1$, Eq. (1) reduces to

$$T^2 \simeq \Omega_l^2\omega_{ci}^2/V_A^2$$

for the eigenmode cutoffs. The relation between the cutoff frequency of a given mode and the electron density is

$$f \simeq A_{lm0}/\eta_e^{1/2} \tag{4}$$

where A_{lm0} is a constant for the (l,m) mode. A set of $k = 0$ dispersion curves is given in Fig. 1.

B. Circuit model of the antenna-cavity coupling

It is well known in microwave theory that the coupling between an antenna and the plasma can be described by circuit models with discrete components. In our experiment, the cavity, i.e., the tokamak, is coupled to the outside system by a loop antenna which is modeled by a transformer. Each of the cavity eigenmodes is described by an RLC resonance circuit. The equivalent circuit of the antenna-cavity system is shown in Fig. 2. Because the antenna is much smaller than the wavelength, the discrete element equivalent circuit is adopted.

From this model, an expression for the input impedance of the antenna Z_L is derived when the various

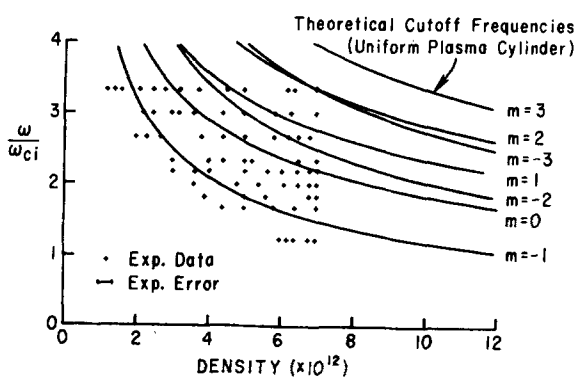

FIG. 1. Theoretical magnetosonic cavity mode cutoffs ($k = 0$) in a cold plasma versus experimental data. These curves are for the $l = 1$ radial mode.

CIRCUIT MODEL OF TOROIDAL EIGENMODES

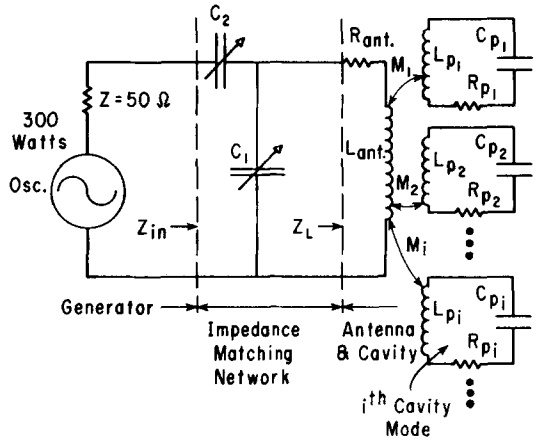

FIG. 2. Circuit model of the antenna-cavity coupling. Each cavity mode is represented by an RLC resonance circuit. M_i is the mutual inductance between the antenna and the ith cavity mode.

eigenmode impedances are reflected into the primary of the transformer. Z_L can be written as

$$Z_L = R_a + j\omega L_a + \sum_i (\omega M_i)^2\left[R_{p_i} + j\left(\omega L_{p_i} - \frac{1}{\omega C_{p_i}}\right)\right]^{-1}, \tag{5}$$

where R_a and L_a are the resistance and inductance of the antenna. It is desirable to rewrite Eq. (5) in terms of the following experimental parameters of

$$Q_{p_i} = \omega_i L_{p_i}/R_{p_i}\,,\quad \omega_i^2 = 1/L_{p_i}C_{p_i}\,,\quad Q_a = \omega L_a/R_a\,,$$

where L_{p_i}, R_{p_i}, and C_{p_i} are the inductance, capacitance, and resistance of the ith cavity mode. Two dimensionless quantities are used, the coupling coefficient κ_i and the normalized frequency Ω_{p_i}:

$$\kappa_i^2 = M_i^2/L_{p_i}L_a\,,\quad \Omega_{p_i} = \omega_i/\omega\,.$$

Near the resonance of the jth cavity mode, the real and imaginary parts of Z_L can be approximated as

$$R_L = R_a\left(1 + \sum_i \frac{Q_a\kappa_i^2 Q_{p_i}\Omega_{p_i}}{\Omega_{p_i}^2 + Q_{p_i}^2(1-\Omega_{p_i}^2)^2}\right), \tag{6}$$

$$X_L = X_a\left(1 - \sum_i \frac{(1-\Omega_{p_i}^2)\kappa_i^2 Q_{p_i}^2}{\Omega_{p_i}^2 + Q_{p_i}^2(1-\Omega_{p_i}^2)^2}\right). \tag{7}$$

At a particular frequency, only the term with a resonance frequency closest to the applied frequency will dominate the resistive loading, whereas the reactance depends on the coupling coefficient and Q of all the other modes. Depending on the magnitudes of the contribution to the input reactance from the modes above and below the resonance frequency, the total reactance from all the cavity modes, $X_L - X_a$, can be greater or less than zero. If the reactance contribution from modes with resonant frequency $\omega_j < \omega_i$ is greater than the contribution from the other modes, for instance, the input reactance X_L will show an increase in the basic antenna inductive reactance from the effects of the cavity modes.

C. Impedance matching

The impedance matching network, consisting of the two tuning capacitors, C_1 and C_2 in Fig. 2, is used to tune out the antenna inductance and to transform the antenna resistance to 50 Ω. For a particular setting of C_1 and C_2, only one value of L_a and R_a can be matched to 50 Ω. Therefore, the conditions under which the antenna is matched must be specified.

Even when there are no cavity resonances present during the discharge, the background plasma causes a sufficient change in the antenna input impedance from its vacuum value so that retuning the antenna is necessary. This kind of tuning will be denoted as "off-resonance" matching. The sum of the "off-resonance" plasma impedance plus the antenna impedance will be denoted $Z_f = R_f + jX_f$.

There is one more type of matching, namely, to match the generator impedance to the impedance of the antenna plus the added contribution from the plasma at one of the resonance peaks. Because the impedance contribution from each of the eigenmodes is different from the others, only one mode can be exactly matched for a particular setting of C_1 and C_2. For future reference, the term "on-resonance" matching is used to denote this type of matching.

In the experiment, the plasma loading impedance Z_L can be calculated from the measured antenna input impedance Z_{in} and the capacitance C_1 and C_2.

D. Antenna coupling coefficient and wave generation efficiency

In order to optimize a heating experiment, it is important to maximize the efficiency of rf power coupled into the tokamak. As shown in Fig. 2, the antenna coupling coefficient κ_i^2 and the wave generation efficiency η can be related to a set of experimental measureable quantities in the following manner:

$$\kappa_i^2 = \frac{R_L/R_a - 1}{Q_{p_i} Q_a}, \tag{8}$$

$$\eta = \kappa_i^2 Q_a Q_{p_i}/(1 + \kappa_i^2 Q_a Q_{p_i}). \tag{9}$$

From the cutoff dispersion relations of the magnetosonic wave [Eq. (4)], the cavity Q can be estimated from the plasma density at a cavity resonance, the rate of density change as a function of time, and the 3 dB time width of the resonance peak

$$Q \simeq 2n_e/\Delta n_e .$$

Such a measurement gives the cavity Q loaded by the strongly coupled input antenna Q_{L_i}. The unloaded Q_{p_i} can be related to the loaded Q_{L_i} for an off-resonantly matched antenna as follows:

$$Q_{p_i} = Q_{L_i}(1 + \omega_i^2 M_i^2/2R_f R_{p_i}). \tag{10}$$

All the terms in this equation can be measured; $\omega_i^2 M_i^2/R_{p_i}$, for instance, is just the loading of the antenna due to the plasma at the peak of a resonance.

E. Simulation of cavity resonances

It is useful to see what general effects the impedance function [Eq. (5)] will predict before actually discussing the experimental results. The essence of the circuit model discussion is that the form of the impedance function observed in the experiment should be reasonably close to the form of Eq. (5). The values of the circuit parameters used in the simulation are either calculated from theory or measured in experiment.

The simulation starts with the equivalent RLC circuits for the resonance cavity. Since the cutoff relation of the eigenmodes is approximately $f \propto 1/n^{1/2}$ and $\omega_{0p} \propto 1/C_p^{1/2}$, where ω_{0p} is the resonance angular frequency of the RLC circuit, the value of the capacitor C_p is assumed to be proportional to the density. For the ith mode, the proportionality between C_p and $n(t)$ is such that $\Omega_{p_i} = 1$ at the ith mode.

The coupling coefficient κ_i^2 and the cavity Q_{p_i} can be estimated from theory.[17] For the sake of simplicity, the values of κ_i^2 and Q_{p_i} used in this simulation are the same for all modes, even though they are actually different for the various modes in the experiment. The results of the simulation for the loading impedance Z_L are shown in Fig. 3. The plasma loading impedance $Z = R + jX$, shown in Fig. 2, is related to Z_L by the relation

$$Z = Z_L - Z_a .$$

A few features of this simulation should be noted for later comparison with experimental data. First, for a simple pole resonance, there is a relation between the real and the imaginary parts of the impedance. Corre-

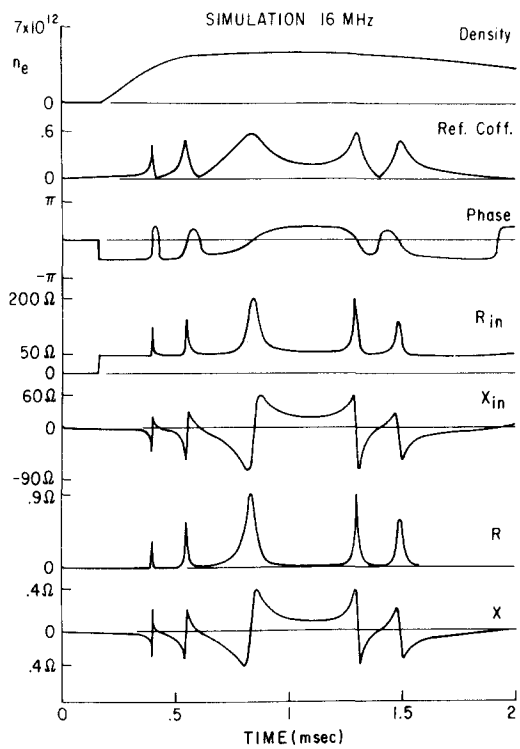

FIG. 3. Computer simulation of various equivalent circuit parameters. In the computation, $Q_a = 100$, $Q_p = 400$, and $\kappa^2 = 8 \times 10^{-5}$.

sponding to every peak in the real part of the impedance, the imaginary part should undergo a steep change. Since the reflection coefficient is related to the impedance by a complex transform, this same behavior should also exist between the amplitude and the phase of the complex reflection coefficient. This point is demonstrated in traces 2–5. Second, the direction of the change of the reactance is a function of the sign of the slope of the density evolution. During the density buildup, the reactance goes negative first, then jumps to a positive value when a resonance is passed through, whereas, during the density decay, the reactance is positive before passing through a resonance. This behavior is shown in traces 5 and 7.

F. Q circles

Another way to see the simple pole resonance effect of a cavity mode is by plotting the input resistance of the cavity against the input reactance in the complex impedance plane. As a cavity resonance is passed through, the resultant curve is a circle, known as a Q circle.[18] Depending on how the resonance is passed through, there is a definite direction in tracing out the Q circle, i.e., clockwise or counterclockwise. The Q circles for the resonances appearing during the density buildup are formed opposite to the direction of rotation for those occurring at the density decay.

III. EXPERIMENTAL APPARATUS

A. Transmission measurement

The magnetosonic cavity modes were first observed with a small six-turn loop probe located 180° toroidally from a transmitting antenna, as shown in Fig. 4. The receiving probe was kept small so that it coupled weakly to the cavity and would not influence the cavity while measuring the rf signal. A single-turn tungsten loop antenna was first used as the transmitting antenna. When it was discovered that the antenna resistance must be minimized in order to detect the plasma loading, the tungsten antenna was replaced by a two-turn copper loop antenna (Appendix).

A 300 W wide-band amplifier was used to excite the magnetosonic wave. The input rf frequency to the transmitting antenna was fixed for each plasma discharge so that only one parameter, the plasma density, was changing during the experiment. To study the frequency dependence of the cavity modes, the input frequency is changed between plasma shots.

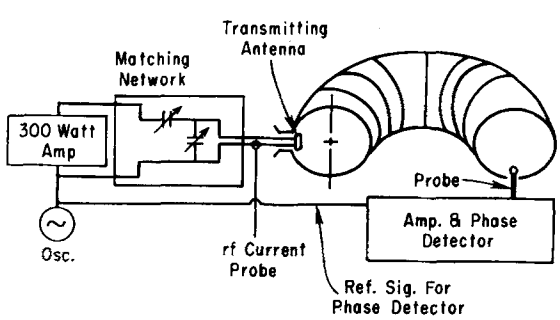

FIG. 4. Experimental arrangement of the transmission measurement.

B. Plasma loading impedance measurement

The plasma loading resistance was obtained by measuring the incident and reflected powers into the antenna, plus the antenna current. Figure 5 shows the experimental setup for the plasma loading measurements. The incident and reflected powers, P_i and P_r, were measured with a directional coupler while the antenna current I was detected with the rf current probe. The plasma loading resistance can be calculated as follows:

$$R=(P_i-P_r)/I^2-R_a. \tag{11}$$

C. Complex plasma loading impedance measurement

To obtain the complex loading impedance of the plasma at a cavity resonance, the phase difference between the incident and the reflected voltage into the antenna was measured. The complex reflection coefficient is obtained from the voltage and phase measurements

$$\rho=|V_r|/|V_i|e^{i\Phi},$$

where V_i and V_r are the incident and reflected voltages and $\phi=\phi_r-\phi_i$ is the phase. The complex antenna input impedance can be calculated from the complex reflection coefficient.

IV. PLASMA PARAMETERS

The Caltech tokamak has a 15 cm minor radius and a 45 cm major radius. The vacuum chamber is constructed of stainless steel without any limiter. The typical plasma parameters for the wave excitation experiments are summarized in Table I.

The vacuum chamber of the Caltech tokamak is cleaned by low power discharge cleaning, first proposed by Taylor,[19] to reduce the loosely bonded impurities (carbon and oxygen) on the chamber wall. The Z_{eff} of the Caltech tokamak plasma is believed to be quite low as a result of the discharge cleaning.

A side effect of the discharge cleaning is that the plasma density drops very quickly after the initial plasma density buildup. As shown in the top trace in Fig. 6, the electron density peaks at 7×10^{12} particles per cm^3 in the first 0.3 msec, then drops to 1×10^{12} particles per cm^3 in the next 2 msec. The consequence of this density behavior on the wave excitation is that no cavity mode can propagate in the Caltech tokamak beyond the first 2 msec in the plasma discharge when the plasma density falls below the cutoff condition of Eq. (4).

V. EXPERIMENTAL RESULTS

A. Transmission measurements

The toroidal eigenmodes were first observed in transmission. At constant input frequency, the cavity modes were swept through by the change in the plasma density as a function of time. The modes appear as a series of peaks on the rf output of the receiving probe located 180° toroidally from the transmitter. The received rf signals were passed through a 300 kHz bandpass filter and then fed into a crystal detector for amplitude detection.

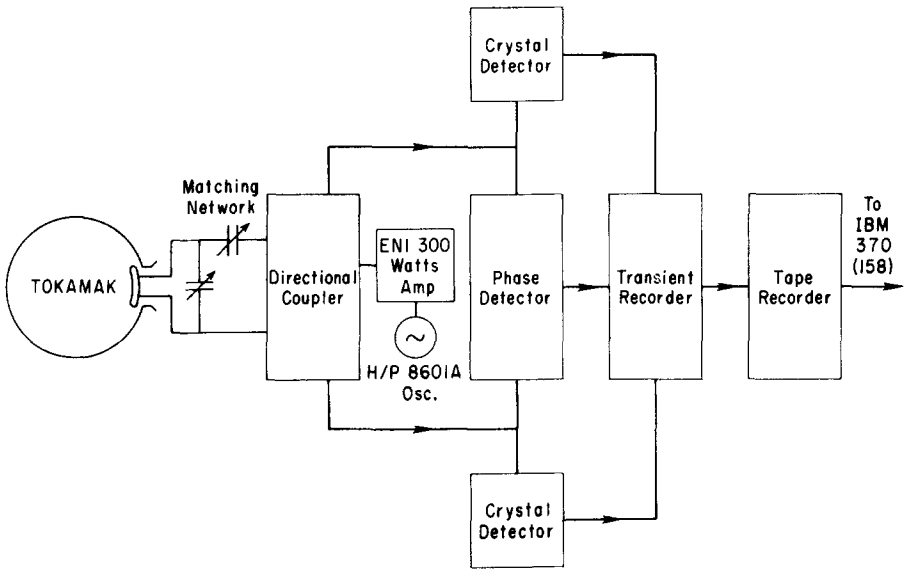

FIG. 5. Data acquisition system for the various experiments.

A few of the typical transmission measurements for various input frequencies are shown in Fig. 6. The top curve is a trace of the electron density evolution as a function of time for a typical plasma discharge.

The density values at which resonance peaks appeared are found to be a function of the applied frequency. At the lower applied frequencies, the transmission peaks cluster near the high density region, whereas they become more spread out into the low density region at higher frequencies. This is the expected behavior from the dispersion relation for the magnetosonic wave.

To compare with the theory for a cold uniform cylindrical plasma-filled cavity model, the cutoff curves for the various poloidal modes are superimposed on the experimental data in a density versus frequency graph (Fig. 1). The agreement between the experimental data and the theory is fairly good, although not perfect. There are data points that fall below the cutoff curves. Some of the discrepancies between theory and experiment are due to the simplicity of the theory used. The toroidal effects, radial density profile, poloidal magnetic field effects, and many others, have not been properly accounted for in the theory. There is also a small amount of uncertainty in the experimental data as indicated in Fig. 1. This comes from the experimental errors in the electron density measurement where the density uncertainty is about $\pm\frac{1}{4}$ fringe at the output of the 65 GHz microwave interferometer.

TABLE I. Plasma parameters for the wave excitation experiments.

Toroidal field:	3 to 6 kG (4 kG on center) at $R=30$ cm and $R=60$ cm, respectively
Plasma current:	15 kA (peak) 12 msec (duration)
Line average electron density: (4 mm microwave)	7×10^{12} to 1.5×10^{12} cm (decay during the first two msec)
Average electron temperature:	50 to 100 eV (assuming $Z_{eff}=1.5$)

B. Background plasma loading impedance

The off-resonance antenna impedance Z_f can be determined from the capacitance values used to match the generator impedance off resonantly. To obtain the background plasma loading ΔZ in the absence of any cavity mode, the antenna impedance must be subtracted from Z_f

$$\Delta Z = Z_f - Z_a .$$

An interesting experimental finding is that the background plasma loading reactance ΔX is greater than zero, indicating that the antenna inductance is increased by the plasma effect. A possible explanation for the increase in the antenna input inductance due to the background plasma has been discussed earlier. As indicated in Eq. (7), if the reactance contribution from the cavity modes with resonant frequencies higher than the applied frequency is greater than the contribution from the other modes, the basic antenna inductive reactance will show an increase. The values of ΔR and ΔX for the different input frequencies are given in Tables I and II.

C. Plasma loading resistance at the cavity resonances

The experimental results of the plasma loading resistance R at the various cavity modes are presented in this section. The plasma loading resistance is obtained from the power-current measurements.

Figure 7 shows a typical plasma discharge, where the input rf frequency is 11 MHz and the antenna is tuned off resonantly. The off-resonance tuning condition is indicated in the reflected voltage data, where the reflected voltage is a minimum between the cavity resonances. When a cavity resonance appears, the generator impedance is no longer matched, and so a cavity resonance shows up as an increase in the reflected voltage and at the same time as a decrease in the antenna current. This relation between the reflected voltage and the antenna current can be understood as follows: Since the incident voltage is relatively constant throughout the plasma discharge, the amplitude of the reflection

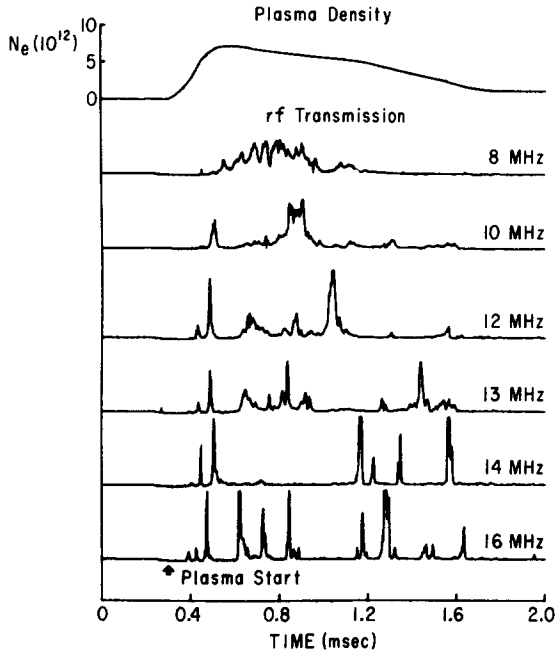

FIG. 6. Transmission measurements versus a typical density evolution as a function of time.

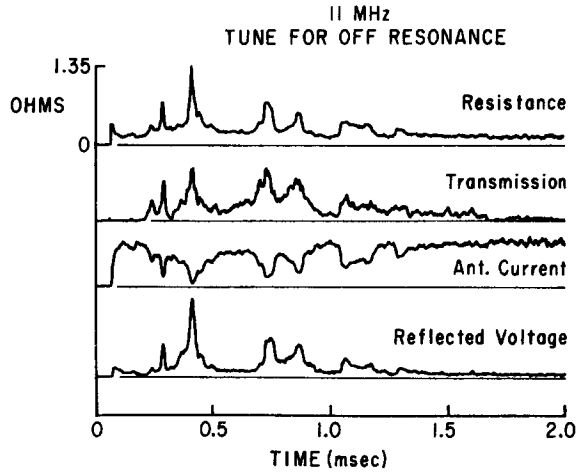

FIG. 7. Calculated plasma loading resistance from input power into the antenna and antenna current data. Antenna is matched to 50 Ω in the absence of cavity resonances.

coefficients, $|\rho| = (V_r/V_i)$, should essentially be proportional to the amplitude of the reflected voltage. The antenna current can be expressed in terms of the reflection coefficient as

$$I = \frac{V}{Z_0}\left(\frac{1-\rho}{1+\rho}\right),$$

where Z_0 is the characteristic line impedance. The denominator $(1+\rho)^{-1}$ can be approximated by $(1-\rho)$ if the mismatch is small; thus, the equation can be written in the following approximate form:

$$I \simeq (V/Z_0)(1-2\rho).$$

From this relation one can see that if there is an increase in the reflected voltage, there must be a corresponding decrease in the antenna current.

The general features of the time dependence of the resonant loading resistance peaks correlate well with the time dependence of the peaks in the transmitted signal. An observation in the experiment is that the modes with the largest transmission amplitude are not necessarily the ones that show the largest input loading resistance. This is because the input loading resistance measures the power delivered into the cavity, whereas the receiving probe only detects one component of the field. Depending on the cavity mode that is excited, strong input loading does not necessarily correspond to a strong field component measured by the probe.

The magnitudes of the plasma loading resistance for the various cavity modes at different input frequencies are summarized in Tables II and III. For each input frequency there are many cavity modes excited, each with a different loading resistance. Therefore, only the range of peak loading resistance for various cavity resonances at each input frequency is given in these tables. This range of the "resonant" loading resistance is denoted by R_I, where the subscript I is to identify the power-current method used to determine the resistance, thus differentiating this result from the loading resistance R_r obtained from the measured complex reflection coefficient. The computed values of R_I and R_r from experimental data are compared in Table IV.

TABLE II. Summary of the plasma loading impedance for "off-resonant" matching condition. R and L are the input resistance and inductance of the antenna measured under various conditions. The top line of each double row is the data taken in vacuum and the second line corresponds to data taken in the plasma. $\Delta R = R_f - R_a$ and $\Delta X_L = X_f - X_a$ are the background plasma loading impedance. R_I is the range of the peak loading resistance obtained by power-current method.

Freq. (MHz)	Condition	C_1(pF)	C_2(pF)	L(μH)	R(Ω)	ΔR(Ω)	ΔX_1(Ω)	R_I(Ω)
10	Vacuum	531	45.7	0.44	0.31			
	Plasma	502	45.0	0.462	0.36	0.05	1.38	0.5–0.9
12	Vacuum	360	36.0	0.445	0.4			
	Plasma	347	38.0	0.46	0.485	0.085	1.13	0.6–1.0
14	Vacuum	270	28.7	0.433	0.456			
	Plasma	225	30.7	0.453	0.57	0.114	1.76	0.8–1.5
16	Vacuum	207	23.5	0.43	0.514			
	Plasma	190	25.0	0.46	0.668	0.154	3.0	0.9–1.2
18	Vacuum	165.8	20.5	0.42	0.6			
	Plasma	148.8	22.0	0.459	0.82	0.22	4.41	0.9–1.2

TABLE III. Summary of another data set taken under conditions similar to that presented in Table II. These data were taken on a different day from those given in Table II.

Freq. (MHz)	Condition	C_1(pF)	C_2(pF)	L(μH)	R(Ω)	ΔR(Ω)	ΔX(Ω)	R_I(Ω)
10	Vacuum	525	44.5	0.445	0.3	0.05		
	Plasma	490	45.2	0.474	0.350	0.05	1.823	0.4 – 0.8
12	Vacuum	364	35.1	0.441	0.38			
	Plasma	352	37.5	0.453	0.456	0.076	0.86	0.8 – 1.2
14	Vacuum	264	27.8	0.444	0.448			
	Plasma	244	28.2	0.476	0.53	0.082	2.77	0.6 – 0.1
16	Vacuum	200	23.9	0.443	0.563			
	Plasma	192	26.0	0.455	0.7	0.137	1.2	0.6 – 1.3
18	Vacuum	161	20.0	0.432	0.604			
	Plasma	150	24.9	0.448	1.0	0.4	1.81	0.7 – 1.2

D. Complex plasma loading impedance measurement

The complex loading impedance is important in determining how to match the generator impedance to one of the cavity resonances. Only by matching the generator impedance to a cavity resonance can the maximum power be delivered to the cavity when the plasma loading is highest.

Experimental results for input frequency of 16 MHz are shown in Fig. 8, and the general behavior of the complex input impedance for the various input frequencies is discussed. The complex impedance data for the various input frequencies are summarized in Table IV.

The first trace in Fig. 8 is the amplitude of the reflection coefficient, calculated from the incident and reflected voltage data. The phase data in trace 2 are the direct output of the phase detector. As expected, corresponding to every peak in the reflected voltage, there is a steep change in the measured phase. From the complex reflection coefficient, the complex input impedance Z_{in} can be calculated (traces 3 and 4). When these data are compared with the calculated values shown in the fourth and fifth traces in Fig. 3, the general features of the data seem to agree well with the computed results from the circuit model. For the experimental data in Fig. 8, the plasma density reaches a maximum at 1 msec into the discharge. At this time, the slope of the density evolution reverses sign, so that as stated before, both the measured phase and the reactance reverse in direction. The measured reactance goes negative before passing through a resonance during the density buildup and goes positive before passing through a resonance during the density decay.

The next step in the calculation is to compute the plasma loading impedance $Z = R + jX$ by transforming Z_{in} across the matching network and subtracting the impedance of the antenna Z_a. The results of the computation are shown in traces 5 and 6 of Fig. 8. The maximum resistive loading is about 1.8 Ω in comparison with 1.2 Ω, obtained from the power-current method. At 16 MHz the antenna resistance is about 0.56 Ω; therefore, the plasma loading is between two and three times the antenna resistance. When the antenna is matched at the cavity resonance, this corresponds to a wave generation efficiency η between 70% and 80%.

When the real and imaginary parts of the impedance are plotted against each other as they pass through a resonance, the resultant curve is a circle, known as the Q circle. Figures 9 and 10 are the experimental Q circles of the two major peaks which occur at time 0.9 msec, and time = 1.1 msec in Fig. 8. The time between the points in the Q circle plots is 2 μsec. They are approximately circles, although there are some distortions. The distortions of the Q circles can be partly

TABLE IV. The ranges of the complex plasma loading impedance, R_{res} and X_{res}, at the various cavity modes are given in columns 8 and 9. The resistive loading at the same cavity modes measured with the power-current method is shown is column 7. C_1 and C_2 are the values of the tuning capacitors. R and L are the antenna resistance and inductance with or without plasma. The data were taken under off-resonant tuning condition and the antenna is 2.6 cm into the tokamak chamber.

Freq. (MHz)	Condition	C_1(pF)	C_2(pF)	L(μH)	R(Ω)	R_I(Ω)	R_{res} (Ω)	X_{res}(Ω)
10	Vacuum	532	44.5	0.44	0.293			
	Plasma	509	46.1	0.457	0.34	0.5 to 0.1	0.6 to 1.1	−0.52 to 0.6
12	Vacuum	364	34.8	0.442	0.375			
	Plasma	352	37	0.453	0.445	0.4 to 0.7	0.75 to 1.1	−0.6 to 0.8
14	Vacuum	262	28.4	0.446	0.472			
	Plasma	256	32	0.45	0.61	0.7 to 1.3	0.9 to 1.46	−0.7 to 1.0
16	Vacuum	199	23	0.446	0.53			
	Plasma	189	27	0.459	0.77	1.0 to 1.5	1.2 to 1.8	−0.8 to 1.2
18	Vacuum	161	20.8	0.43	0.65			
	Plasma	146	24	0.461	0.98	0.8 to 1.7	0.95 to 2	−0.9 to 0.8

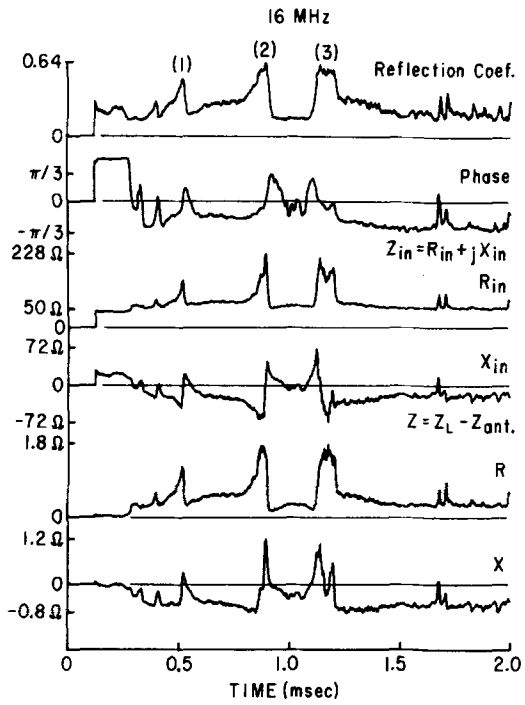

FIG. 8. Computed complex plasma loading impedance from the complex reflection coefficient. The three identified peaks correspond to the two Q circles shown in Figs. 9 and 10.

attributed to errors in the calibration of the square law crystal detector, the linear phase detector, and partly to density fluctuations. The effects of the density fluctuations are most pronounced in Fig. 10 where small oscillating points are superimposed on the main circular curve. The peak occurring in the density buildup is traced out counterclockwise as shown in Fig. 9, while the resonance shown in Fig. 10 is traced out in the clockwise direction during the density decay. This behavior is what the circuit model has demonstrated.

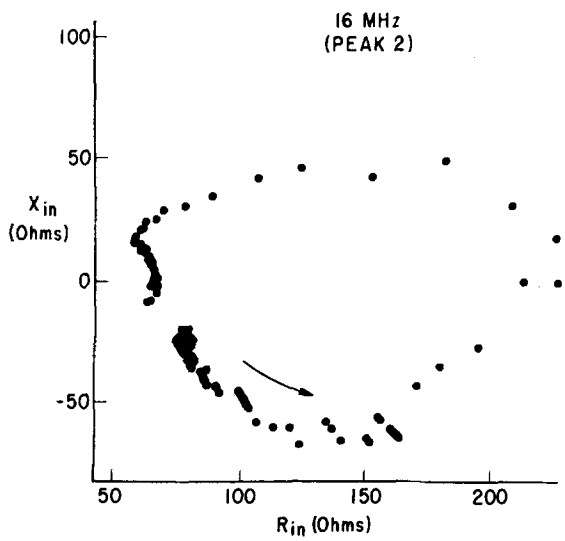

FIG. 9. Q circle for the second peak shown in Fig. 11. The circle is traced out counterclockwise, and the time between consecutive points is 2 μsec.

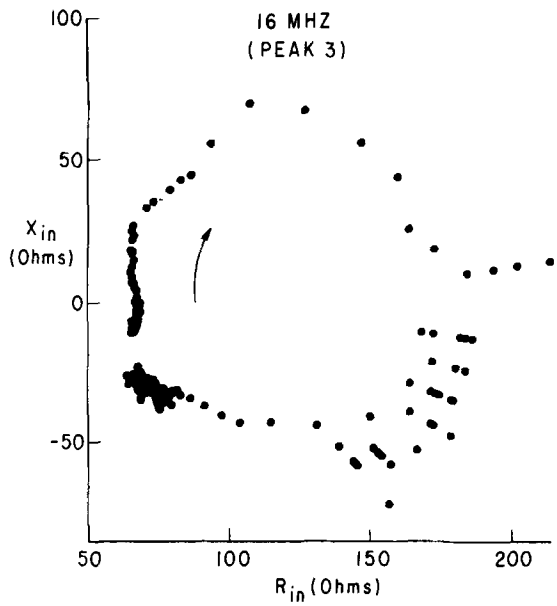

FIG. 10. Q circle for the third peak shown in Fig. 11. The circle is traced out clockwise, and the time between consecutive points is 2 μsec.

E. Cavity Q, antenna coupling coefficient, and antenna efficiency

By using the approximate density-frequency relation for the cavity mode cutoffs, the Q of the plasma-filled cavity can be simply estimated. The unloaded Q of the cavity can be related to the measured loaded Q_L by Eq. (10). Q_L, Q_0, the antenna coupling coefficient, and the wave generation efficiency for the three major resonance peaks of Fig. 8 are given in Table V.

It must be emphasized that this method of calculating Q of the cavity is only an estimation. Furthermore, there is an experimental error in the measured density; that is, there is an uncertainty factor of $\pm\frac{1}{4}$ fringe in the density measurement with the microwave interferometer. The estimated Q's for the cavity resonances with different input frequencies do not differ greatly. For the frequency range used in the experiment, between 10 and 16 MHz, the range of the loaded Q is between 120 and 150, and the range of the unloaded Q is between 400 and 700.

The contribution to the measured cavity Q can be divided into two parts: (i) the damping of the wave by the plasma and (ii) the energy losses due to the finite conductivity of the tokamak wall which is made of stainless

TABLE V. The estimated loaded Q, unloaded Q, antenna coupling coefficient, and the antenna efficiency for the three resonance peaks shown in Fig. 11. The antenna Q_a used in the computation is 90.

Cavity resonance peaks	Loaded cavity Q (Q_L)	Unloaded cavity Q (Q_0)	Coupling coefficient (κ^2)	Antenna efficiency (η)
1	240	470	5.6×10^{-5}	70%
2	240	560	6.5×10^{-5}	77%
3	170	400	8.3×10^{-5}	75%

steel. It is important here to estimate the losses in the tokamak wall to see whether the wall loss is a dominant factor. The calculated cavity Q of $(m=0,\ l=1,\ k=0)$ mode for a cold plasma-filled cylindrical cavity with a stainless steel wall is about 1300. This is two to three times higher than the Q of the measured cavity. Therefore, although the wall loss is not small, it is not the dominant term in the measured cavity Q, and so a large part of the wave energy should be absorbed by the plasma.

The coupling coefficient is a function of the distance that the antenna protruded into the vacuum chamber (see the Appendix). For the different cavity modes at various input frequencies, the coupling coefficient of the antenna when it is 2.6 cm into the tokamak chamber has a range between 3×10^{-5} and 1×10^{-4}.

F. Matching impedance at the cavity resonances

For future high power experiments, it is essential to be able to match the generator impedance at one of the cavity resonances where the resistive loading of the cavity is high. This process is much more difficult than matching off resonantly because during the passage through of a resonance, both the real and imaginary parts of the impedance are changing very fast.

One of the on resonantly tuned cases is given in Fig. 11. As indicated before, only one mode is properly matched for each case. The experimental data of the reflected voltage and rf current on-resonant matching experiment appear just opposite to the data from the off-resonant tuning experiment.

VI. CONCLUSIONS

This paper has presented the results of some low power experiments in the propagation of the fast magnetosonic cavity modes in a research tokamak. A great deal of attention has been given to the study of the complex input impedance of the antenna, the antenna design, and the design of the impedance matching network. These measurements are of great importance to future high power experiments where efficient coupling of power to the plasma is essential. Through the high power heating experiments, the feasibility of using magnetosonic waves as a method to heat the plasma to fusion ignition can be evaluated.

The general conclusions for these experiments are that the possibility for efficient power coupling into the plasma-filled cavity looks very encouraging because of the reasonable plasma loading resistance found at the cavity resonances. The matching of the generator impedance to the antenna impedance at resonance does not seem to be a serious problem. The loading resistance at the cavity modes has been observed to be as high as three to four times the antenna resistance, and the generator impedance has been matched to a few of the cavity modes. This means that with the present antenna design, as much as 80% of the power can be delivered into the tokamak via the cavity resonances, and only 20% of the input power will be lost in the antenna. To further increase the wave generation efficiency, it is necessary to increase both the antenna Q and its coupling coefficient.

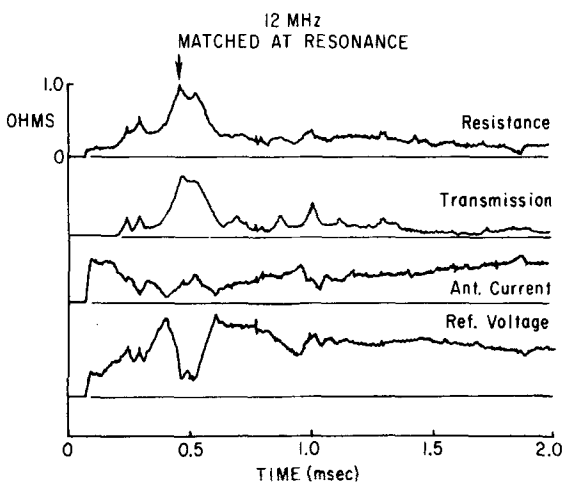

FIG. 11. Antenna is matched to one of the cavity resonances.

ACKNOWLEDGMENTS

One of the authors (DQH) would like to express his appreciation to Dr. W. Bridges, Dr. J. Long, and Dr. H. Martel for the many useful discussions and suggestions.

Special thanks go to F. Cosso for his skillful assistance in constructing the experimental instruments.

This work was supported by the U. S. Department of Energy Contract AT(04-3) 767, Project Agreement No. 2.

APPENDIX: TRANSMITTING ANTENNA

The transmitting antenna is a two-turn loop made of 0.32 cm copper tubing which is enclosed in a 0.08 cm thick coat of Pyrex insulator. The functions of the glass are to protect the copper from plasma damage and to electrically insulate the antenna from the plasma. The approximate loop area of the antenna is 8.9 cm by 2.54 cm. Because of the glass coating, the antenna never intrudes more than 3.2 cm into the tokamak vacuum chamber (Fig. 12). The ultimate limitation on the antenna size and the feed-through length is determined by the tokamak port size which is $10\times15.3\times2.54$ cm.

The antenna resistance and inductance are a function of the distance that the antenna protrudes into the vac-

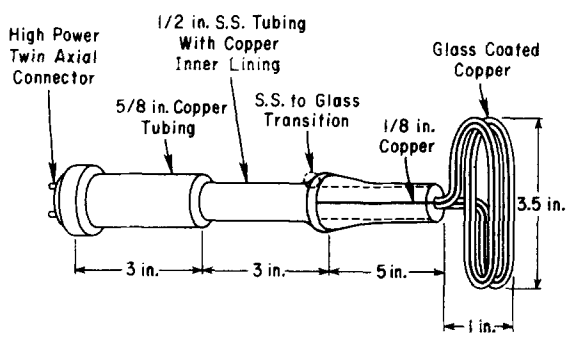

FIG. 12. Design of the two-turn copper antenna.

uum chamber of the tokamak. The reason for this dependence on the distance into the vacuum chamber is because of the $15.3 \times 10 \times 2.54$ cm stainless steel port where the antenna sits when it is completely outside the tokamak vacuum chamber. The effect of the stainless steel port is to lower the antenna inductance and increase the antenna resistance through eddy current losses in the port wall.

The antenna inductance measured in the experiment is approximately 0.45 μH and independent of the input frequency. The antenna resistance is about 0.4 Ω and has a square-root dependence on the input frequency. This is the expected frequency dependence from skin effect calculations.

[1]H. Eubank, R. Goldston, V. Arunasalam, M. Bitter, K. Bol, D. Boyd, N. Bretz, J. P. Bussac, S. Cohen, P. Colestock, S. Davis, D. Dimock, H. Dylla, P. Efthimion, L. Grisham, R. Hawryluk, K. Hill, E. Hinnov, J. Hosea, H. Hsuan, D. Johnson, G. Martin, S. Medley, E. Meservey, N. Sauthoff, G. Schilling, J. Schivell, G. Schmidt, F. Stauffer, L. Stewart, W. Stodiek, R. Stooksberry, J. Strachan, S. Suckewer, H. Takahashi, G. Tait, M. Ulrickson, S. von Goeler, and M. Yamada, in *Plasma Physics and Controlled Nuclear Fusion Research* (International Atomic Energy Agency, Vienna, 1979), Vol. I, p. 167.

[2]T. H. Stix, *The Theory of Plasma Waves* (McGraw-Hill, New York, 1962), Chap. 5.

[3]J. Adam and A. Samain, in Report EUR-CEA-FC-579 (1971), p. 29.

[4]F. W. Perkins, M. Chance, and J. E. Kindel, in *Proceedings of the Third International Symposium on Toroidal Plasma Confinement* (Max-Planck-Institut für *Physik*, Garching, Germany, (1973), paper B8.

[5]J. C. Hosea and R. M. Sinclair, Phys. Fluids **13**, 701 (1970).

[6]F. Paoloni, Phys. Fluids **18**, 640 (1975).

[7]D. G. Swanson, Phys. Fluids **17**, 2241 (1974).

[8]TFR Group, in *Proceedings of the Third International Meeting on Theoretical and Experimental Aspects of Heating of Toroidal Plasmas* (Pergamon, New York, 1978), Vol. I, p. 87.

[9]W. M. Hooke, M. A. Rothman, P. Avivi, and J. Adam, Phys. Fluids **5**, 864 (1962).

[10]D. G. Swanson, R. W. Gould, and R. H. Hertel, Phys. Fluids **7**, 269 (1964).

[11]K. Chung and M. A. Rothman, Phys. Fluids **10**, 2634 (1967).

[12]V. L. Vdovin, O. A. Zinoviev, A. A. Ivanov, L. L. Kozorovitskii, M. F. Krotov, V. V. Parail, Ya. R. Raksimbabaev, V. D. Rusanov, and V. Shapotkovski, Zh. Eksp. Teor. Fiz. Pis'ma Red. **14**, 149 (1973) [JETP Lett. **17**, 2 (1973)].

[13]N. V. Ivanov, I. A. Kovan, and E. V. Los' Zh. Eksp. Teor. Fiz. Pis'ma Red. **14**, 138 (1971) [JETP Lett. **16**, 60 (1972)].

[14]J. C. Hosea, W. M. Hooke, Phys. Rev. Lett. **31**, 150 (1973). Also, J. Adam, M. Chance, H. Eubank, W. Getty, E. Hinnov, W. Hooke, J. Hosea, F. Jobes, F. Perkins, R. Sinclair, J. Sperling, and H. Takahashi, in *Plasma Physics and Controlled Nuclear Fusion Research*, (International Atomic Energy Agency, Vienna, 1974), Vol. I, p. 65.

[15]H. Takahashi, C. Daughney, R. Ellis, R. Goldston, H. Hsuan, T. Hagashima, F. Paoloni, A. Sivo, and S. Suckewer, Phys. Rev. Lett. **39**, 31 (1977).

[16]TFR Group, in *Plasma Physics and Controlled Nuclear Fusion Research* (International Atomic Energy Agency, Vienna, 1977), Vol. III, p. 39.

[17]F. Paoloni, Princeton Plasma Physics Laboratory Report MATT-1173 (1975); F. Paoloni, Nucl. Fusion **18**, 359 (1978).

[18]E. L. Ginzton, *Microwave Measurements* (McGraw-Hill, New York, 1957), Chap. 9.

[19]L. Oren and R. J. Taylor, Nucl. Fusion **17**, 1143 (1977).